

University of Massachusetts Medical School

eScholarship@UMMS

Radiology Publications

Radiology

2020-08-20


Extracellular Vesicles from *Pseudomonas aeruginosa* Suppress MHC-Related Molecules in Human Lung Macrophages

David A. Armstrong
Dartmouth-Hitchcock Medical Center

Et al.

Let us know how access to this document benefits you.

Follow this and additional works at: https://escholarship.umassmed.edu/radiology_pubs

 Part of the [Bacteria Commons](#), [Bacterial Infections and Mycoses Commons](#), [Cell Biology Commons](#), [Immunology and Infectious Disease Commons](#), [Microbiology Commons](#), and the [Respiratory Tract Diseases Commons](#)

Repository Citation

Armstrong DA, Lee MK, Hazlett HF, Dessaint JA, Mellinger DL, Aridgides DS, Hendricks GM, Abdalla MA, Christensen BC, Ashare A. (2020). Extracellular Vesicles from *Pseudomonas aeruginosa* Suppress MHC-Related Molecules in Human Lung Macrophages. *Radiology Publications*. <https://doi.org/10.4049/immunohorizons.2000026>. Retrieved from https://escholarship.umassmed.edu/radiology_pubs/561

Creative Commons License



This work is licensed under a [Creative Commons Attribution-NonCommercial 4.0 License](#)

This material is brought to you by eScholarship@UMMS. It has been accepted for inclusion in *Radiology Publications* by an authorized administrator of eScholarship@UMMS. For more information, please contact Lisa.Palmer@umassmed.edu.

Extracellular Vesicles from *Pseudomonas aeruginosa* Suppress MHC-Related Molecules in Human Lung Macrophages

David A. Armstrong, Min Kyung Lee, Haley F. Hazlett, John A. Dessaint, Diane L. Mellinger, Daniel S. Aridgides, Gregory M. Hendricks, Moemen A. K. Abdalla, Brock C. Christensen and Alix Ashare

ImmunoHorizons 2020, 4 (8) 508-519

doi: <https://doi.org/10.4049/immunohorizons.2000026>

<http://www.immunohorizons.org/content/4/8/508>

This information is current as of November 5, 2020.

Supplementary Material <http://www.immunohorizons.org/content/suppl/2020/08/20/4.8.508.DCSupplemental>

References This article **cites 56 articles**, 11 of which you can access for free at: <http://www.immunohorizons.org/content/4/8/508.full#ref-list-1>

Email Alerts Receive free email-alerts when new articles cite this article. Sign up at: <http://www.immunohorizons.org/alerts>

Extracellular Vesicles from *Pseudomonas aeruginosa* Suppress MHC-Related Molecules in Human Lung Macrophages

David A. Armstrong,^{*,1} Min Kyung Lee,^{†,‡,1} Haley F. Hazlett,[§] John A. Dessaint,^{*} Diane L. Mellinger,^{*} Daniel S. Aridgides,^{*} Gregory M. Hendricks,[¶] Moemen A. K. Abdalla,^{||} Brock C. Christensen,^{†,‡,#} and Alix Ashare^{*,‡}

^{*}Department of Medicine, Dartmouth-Hitchcock Medical Center, Lebanon, NH 03756; [†]Department of Epidemiology, Geisel School of Medicine at Dartmouth, Lebanon, NH 03756; [‡]Department of Molecular and Systems Biology, Geisel School of Medicine at Dartmouth, Lebanon, NH 03756; [§]Department of Microbiology and Immunology, Geisel School of Medicine at Dartmouth, Hanover, NH 03755; [¶]Department of Cell and Developmental Biology, University of Massachusetts Medical School, Worcester, MA 01655; ^{||}Department of Biochemistry, Faculty of Science, Alexandria University, Alexandria 21526, Egypt; and [#]Department of Community and Family Medicine, Geisel School of Medicine at Dartmouth, Lebanon, NH 03756

ABSTRACT

Pseudomonas aeruginosa, a Gram-negative bacterium, is one of the most common pathogens colonizing the lungs of cystic fibrosis patients. *P. aeruginosa* secrete extracellular vesicles (EVs) that contain LPS and other virulence factors that modulate the host's innate immune response, leading to an increased local proinflammatory response and reduced pathogen clearance, resulting in chronic infection and ultimately poor patient outcomes. Lung macrophages are the first line of defense in the airway innate immune response to pathogens. Proper host response to bacterial infection requires communication between APC and T cells, ultimately leading to pathogen clearance. In this study, we investigate whether EVs secreted from *P. aeruginosa* alter MHC Ag expression in lung macrophages, thereby potentially contributing to decreased pathogen clearance. Primary lung macrophages from human subjects were collected via bronchoalveolar lavage and exposed to EVs isolated from *P. aeruginosa* in vitro. Gene expression was measured with the NanoString nCounter gene expression assay. DNA methylation was measured with the EPIC array platform to assess changes in methylation. *P. aeruginosa* EVs suppress the expression of 11 different MHC-associated molecules in lung macrophages. Additionally, we show reduced DNA methylation in a regulatory region of gene complement factor B (*CFB*) as the possible driving mechanism of widespread MHC gene suppression. Our results demonstrate MHC molecule downregulation by *P. aeruginosa*-derived EVs in lung macrophages, which is consistent with an immune evasion strategy employed by a prokaryote in a host-pathogen interaction, potentially leading to decreased pulmonary bacterial clearance. *ImmunoHorizons*, 2020, 4: 508–519.

Received for publication April 17, 2020. Accepted for publication August 1, 2020.

Address correspondence and reprint requests to: David A. Armstrong, Dartmouth-Hitchcock Medical Center, 1 Medical Center Drive, Borwell 508E, Lebanon, NH 03756. E-mail address: david.a.armstrong@hitchcock.org

ORCID: 0000-0003-1748-2520 (D.A.A.); 0000-0002-6132-6472 (D.S.A.); 0000-0003-3022-426X (B.C.C.).

¹D.A.A. and M.K.L. contributed equally to this manuscript.

The microarray data presented in this article have been submitted to the Gene Expression Omnibus (<https://www.ncbi.nlm.nih.gov/geo/>) under accession number GSE142801.

This work was supported by National Institutes of Health (NIH) R01HL122372 (to A.A.) and NIH R01CA216265 (to B.C.C.). Subject enrollment and clinical sample collection were achieved with the assistance of the Cystic Fibrosis Translational Research Core at Dartmouth, which is jointly funded by the NIH (P30DK117469 to Dean Madden) and the Cystic Fibrosis Foundation (STANTO19R0 to Bruce Stanton). The Electron Microscopy Core Facility at the University of Massachusetts Medical School is funded in part by Award S10 OD025113-01 from the National Center for Research Resources, NIH. The funders (Dean Madden and Bruce Stanton) had no role in study design, data collection and analysis, decision to publish, or preparation of the manuscript.

Abbreviations used in this article: CF, cystic fibrosis; *CFB*, complement factor B; CFTR, CF transmembrane conductance regulator; cryo, cryogenic; CTSS, cathepsin S; EV, extracellular vesicle; MS, mass spectrometry; NTA, Nanoparticle Tracking Analysis; TEM, transmission electron microscopy.

The online version of this article contains supplemental material.

This article is distributed under the terms of the [CC BY-NC 4.0 Unported license](https://creativecommons.org/licenses/by-nc/4.0/).

Copyright © 2020 The Authors

INTRODUCTION

Cystic fibrosis (CF) is the most common fatal genetic disease that occurs in whites (1), with nearly 30,000 individuals diagnosed in the United States and an estimated 70,000 individuals afflicted worldwide (2). CF manifests predominantly as a pulmonary disease but also affects gastrointestinal, endocrine/exocrine, and reproductive function. CF is caused by a mutation in a gene that encodes the CF transmembrane conductance regulator (CFTR), a chloride and bicarbonate ion transport channel that maintains osmotic balance across multiple epithelial surfaces in the body (3, 4). Ultimately, 90% of deaths in CF patients are attributed to pulmonary dysfunction directly associated with chronic infection, underscoring the absolute importance of studying the pathogenesis of CF-relevant microbes (5).

P. aeruginosa is an opportunistic pathogen that commonly colonizes the lung in CF patients, resulting in an accelerated decline of pulmonary function (6).

P. aeruginosa is the most dominant pathogen of the lung microbiota of adult CF patients and commonly infects pediatric CF patients (7). Chronic infection with Gram-negative pathogens of CF, including *P. aeruginosa* and *Burkholderia cepacia*, is associated with a rapid decline in pulmonary function, more frequent exacerbations, and higher rates of mortality (8). *P. aeruginosa* resides primarily in the mucus overlying lung epithelial cells and secretes extracellular vesicles (EVs) that diffuse through the mucus and fuse with airway cells, thus delivering virulence factors and other toxins into the host cell cytoplasm that modify the innate immune response (9–14).

EVs are lipid bilayer vesicles secreted by most eukaryotic and many prokaryotic cells and thought to be intimately involved in *trans*-kingdom cross-talk (13, 15–17). EVs can range in size from 20 to 1000 nm, depending on the producing cell and its environment (18). Gram-negative bacterial EVs contain LPS, a known virulence factor, on their surface (19). Moreover, it has been suggested that microbial EVs have important and underappreciated roles in intrakingdom and interkingdom communication by regulating gene expression in target cells directly and indirectly via host immune receptor signaling (18).

Ag presentation is crucial for immune responses. MHC molecules present peptides to other immune cells to mount an adaptive immune response (20). The host response to bacterial infection requires communication between APC and T cells. This communication is relayed through MHC class II Ag presentation to Th cells, followed by adaptive T cell or B cell responses (21). The interaction between T cells and MHC class II, along with the surrounding milieu, is essential for defining the phenotype and success of the inflammatory response to infection.

Macrophages are a key APC of the lung and possess remarkable immune plasticity, with the ability to sense and adapt to the local microenvironment (22, 23). Lung macrophages play pivotal roles in bacterial recognition and elimination as well as in polarization of innate and adaptive immunity. Depending on the local setting, macrophages sometimes play a role in anti-inflammatory responses, tissue repair, and homeostasis, whereas at other times,

they promote inflammatory and phagocytic processes through the complex production of cytokines and cellular interaction (24, 25).

Numerous pathogens employ a strategy of host immune escape during infection, including MHC molecule modulation (26–29). EVs from the periodontal Gram-negative pathogen, *Porphyromonas gingivalis* have been shown to inhibit surface expression of HLA-DR molecules in human umbilical cord vascular endothelial cells (30). Additionally, CFTR inhibitory factor (Cif) protein, a bacterial virulence factor secreted in EVs by *P. aeruginosa*, has been shown to inhibit MHC class I Ag presentation in airway epithelial cells (10).

The goal of this study is to assess whether EVs isolated from one of the most prevalent CF pathogens, *P. aeruginosa*, can alter expression of MHC-related molecules in lung macrophages, thereby potentially modulating the macrophages' ability to mount a proper immune response to the infection.

MATERIALS AND METHODS

This study was approved by the Dartmouth-Hitchcock Institutional Review Board (no. 22781). All subjects were healthy nonsmokers. A total of seven subjects were used in the gene expression portion of this study (three males and four females), with a mean age of 27.14 (± 2.9) y. Lung macrophages from an additional four healthy subjects were used for the protein validation portion of the study (three females and one male), with a mean age 28.25 (± 3.4) y.

Bronchoalveolar lavage and macrophage isolation

Subjects underwent flexible bronchoscopy following local anesthesia with lidocaine to the posterior pharynx and distal trachea/carina with or without i.v. sedation per patient preference. A bronchoscope was inserted *trans*-orally and advanced through the vocal cords. Bronchoalveolar lavage fluid was obtained from tertiary airways via rinses with 20 ml of sterile saline followed by 10 ml of air and repeated for a total of five times per airway. Lung macrophages were isolated as previously described (31, 32).

EV generation and isolation

A clinically derived mucoid strain of *P. aeruginosa* (DH1137, gift from Dr. D. Hogan, Geisel School of Medicine at Dartmouth) was grown overnight (20 h) in Luria–Bertani media. Whole cells were pelleted five times ($3500 \times g$ 20 min) then filtered (0.22 μM), leaving conditioned media containing the EVs. Media was adjusted to pH 4.0. Isolation of EVs was performed by mixing 600 μl of Resin Slurry E (Norgen Biotek, Thorold, ON, Canada) with conditioned media, multiple inversions with a 10-min equilibration. Resin was pelleted with centrifugation at $800 \times g$ for 10 min (Sorvall Legend \times IR Benchtop Centrifuge), media was discarded, and the tube was inverted to drain. To recover EVs, 500 μl of $1 \times$ PBS (pH 6.0) was added to resin, tube was vortexed and allowed a 10 min equilibration, and subsequently centrifuged at $400 \times g$ for 10 min to pellet the resin. PBS containing EVs was centrifuged

two additional times ($400 \times g$ 10 min) to remove any residual resin. EVs in $1 \times$ PBS were aliquoted and stored at -80°C until use.

EV characterization

Negative staining transmission electron microscopy (TEM) was done as previously described (33). Briefly, a $10\text{-}\mu\text{l}$ aliquot of EVs in $1 \times$ PBS was placed on top of carbon-coated formvar support film on 300 mesh Cu grids (Electron Microscopy Science) for 1 min, with excess liquid removed by blotting with filter paper. Sample was immediately stained with 1% uranyl acetate, blotted, and air-dried in a humidity-controlled chamber. The samples were examined using an FEI (Thermo Fisher Scientific) Tecnai 12, transmission electron microscope with an accelerating voltage of 120 KV and images recorded using Digital Micrograph software via a Gatan, Rio9 digital camera system. Cryogenic (cryo)-EV samples were prepared on freshly glow-discharged C-flat copper grids (Electron Microscopy Sciences), plunged into liquid nitrogen cooled, liquified ethane, and stored in liquid nitrogen using an FEI (Thermo Fisher Scientific) Vitrobot set to 2- and 4-s blotting times. Cryo-TEM was carried out on a Phillips CM120 Cryo-TEM at 120 KV accelerating voltage. Images were collected under low-dose conditions using Digital Micrograph software and a Gatan, Orius 4K digital camera system.

Nanoparticle Tracking Analysis (NTA) with the NanoSight NS300 instrument (Malvern, Worcestershire, U.K.) was used to determine mean EV particle size and concentrations as previously described (34). For NTA, EV samples were diluted in PBS and introduced into the sample chamber via syringe pump. The following script was used for EV measurements: PRIME, DELAY 120, CAPTURE 30, and REPEAT 3. Other acquisition settings included the following: camera level of 14, camera shutter speed 13 ms, camera gain 360, and laser blue 488. NTA postacquisition settings were optimized and kept constant between samples. Software used was NTA version 3.2 Dev. Build 3.2.16.

Experimental design and gene expression

Right upper lobe lung macrophages were used in this study, as several studies have shown that the right upper lobe is the predominant lung lobe affected in CF patients (26, 35), and our previous work has shown regional differences in the phenotype of lung macrophages (36, 37). Cells were plated in six-well tissue culture dishes seeded at 1×10^6 cells per well. Cells were allowed to adhere for 60 min, followed by incubation in the presence or absence (negative control) of *P. aeruginosa* EVs at a ratio of 100:1 (EVs/cell), per Cecil et al. (38), for up to 48 h. We have used the 48-h time point to simulate chronic infection. Control experiments were performed as above, in the presence or absence of *Pseudomonas*-derived LPS only (1000 ng/ml). RNA was isolated via RNeasy Mini Kit (QIAGEN, Germantown, MD), as outlined in the manufacturer's instructions, and quantitated on a Qubit 3.0 Fluorometer (Life Technologies, Carlsbad, CA). The digital multiplexed NanoString nCounter human v3 Cancer/Immune RNA expression assay (NanoString Technologies, Seattle, WA) was performed according to the manufacturer's instructions with total RNA. Briefly, 200 ng total RNA was assayed by overnight

hybridization (65°C) with nCounter gene-specific reporter and capture probes. Following a 20-h hybridization, reporter and capture probes are washed away using the automated nCounter Sample Prep Station and probe/target complexes are aligned and immobilized in the nCounter Cartridge. Cartridges are then placed in the nCounter digital analyzer for data collection. nSolver Analysis software (NanoString, V3.0) was used for data analysis including background correction by subtracting the mean of the six negative controls included on the NanoString platform and normalization using the average geometric mean of the 30 housekeeping genes included in the assay.

Immunoblotting

Total protein was obtained by lysing cells in $200 \mu\text{l/well}$ $2 \times$ Laemmli buffer with 5% 2-ME with 1% protease inhibitors and boiling 97°C , 5 min. Lysates were run on 7.5 and 10% gels and transferred to polyvinylidene difluoride membranes. Membranes were washed in Tris-buffered saline with 0.1% Tween 20, cut, and incubated overnight at 4°C in 5% BSA containing 1:5000 primary unless otherwise noted. Primary Abs were the following: monoclonal mouse anti- β -actin (catalog no. ab8226; Abcam), monoclonal rabbit anti-CD14 (catalog no. 56082S; Cell Signaling Technology), 1:2000 monoclonal mouse anti-CD74 (catalog no. sc-20062; Santa Cruz Biotechnology), monoclonal rabbit anti-HLA-DRA (catalog no. 97971T; Cell Signaling Technology), and monoclonal rabbit anti-CD9 (catalog no. 13174S; Cell Signaling Technology). Membranes were then washed four times in TBST and incubated at room temperature for 1 h in BSA-TBST containing 1:5000 secondary. Secondary Abs were the following: mouse IgGk-binding protein (catalog no. sc-516102; Santa Cruz Biotechnology) and polyclonal goat anti-rabbit IgG (catalog no. ab7090; Abcam). Membranes were then washed, exposed to Chemiluminescent Substrate (Thermo Fisher Scientific), and imaged using x-ray film.

Mass spectrometry

Sample was lysed in 8 M urea and 50 mM Tris HCl (pH 8.0) containing $1 \times$ Roche Complete Protease Inhibitor. Lysates were quantified by Qubit fluorometry (Life Technologies). A $20\text{-}\mu\text{g}$ aliquot of each sample was digested in solution using the following protocol: sample was diluted in 25 mM ammonium bicarbonate, and proteins were reduced with 10 mM DTT at 60°C , followed by alkylation with 50 mM iodoacetamide at room temperature. Proteins were digested with $1 \mu\text{g}$ trypsin (Promega) at 37°C for 18 h. The digest was quenched with formic acid and peptides cleaned using solid-phase extraction using the Empore C18 plate (3 M). A $2\text{-}\mu\text{g}$ aliquot was analyzed by nano liquid chromatography/mass spectrometry (MS)/MS with a Waters NanoAcquity HPLC system interfaced to a Thermo Fisher Scientific Fusion Lumos mass spectrometer. Peptides were loaded on a trapping column and eluted over a $75\text{-}\mu\text{m}$ analytical column at 350 nl/min; both columns were packed with Luna C18 resin (Phenomenex) with a 60-min gradient. The mass spectrometer was operated in data-dependent mode, with MS and MS/MS performed in the Orbitrap at 60,000 full width at half maximum resolution and 50,000 full width at

half maximum resolution, respectively. A 3-s cycle time was employed for all steps. Data were searched using a local copy of Mascot with the following parameters: enzyme, trypsin; database, Uniprot-*P. aeruginosa* strain American Type Culture Collection 15692 (forward- and reverse-appended with common contaminants); fixed modification, carbamidomethyl (C); and variable modifications, oxidation (M), acetyl (protein N-term), deamidation (NQ), and pyro-Glu (N-term Q).

Mass values were the following: monoisotopic/peptide mass tolerance, 10 ppm; fragment mass tolerance, 0.02 Da; and max missed cleavages, 2. Mascot DAT files were parsed into the Scaffold software for validation and filtering and to create a nonredundant list per sample. Data were filtered 1% protein and peptide level false discovery rate and requiring at least two unique peptides per protein.

DNA methylation array

Epigenome-wide DNA methylation profiling was performed via the Infinium Methylation EPIC Bead Chips (Illumina, San Diego, CA) for the determination of methylation levels of more than 850,000 CpG sites, as previously described (39). Briefly, DNA was extracted from bronchoalveolar lavage-derived cells via Qiagen DNeasy Blood and Tissue Kit. DNA was quantitated on a Qubit 3.0 Fluorometer (Life Technologies). Bisulfite conversion of DNA was carried out with the Zymo EZ DNA methylation kit (Zymo

Research, Irvine, CA), and EPIC array hybridization and scanning were performed at the University of Southern California Molecular Genomics Core.

DNA methylation array data processing

Raw intensity data files from the MethylationEPIC BeadChips were processed by the *minfi* R/Bioconductor analysis pipeline (version 1.30) (40) with annotation file version *ilm10b4.hg19*. Probes known to cross-hybridize; probes associated with known single-nucleotide polymorphisms, non-CpGs, and sex chromosomes; and probes failing to meet a detection *p* value of 0.05 in $\geq 20\%$ samples were excluded. Location of CpGs were determined by the method of Zhou et al. (41). Genomic contexts and CpG relation to CpG islands were provided in the Illumina EPIC annotation file. The promoter transcriptional context was defined as either having a TSS200 or TSS1500 annotation, or both, in the column *UCSC_RefGene_Group* (transcription start site). CpGs in the promoter context were any with either Promoter_Associated or Promoter_Associated_Cell_type_specific in the *Regulatory_Feature_Group* annotation. Likewise, the gene body transcriptional context was defined as having a body in the *UCSF RefGene Group* annotation. The enhancer context was defined as having a FANTOM5 enhancer record. DNA methylation array data have been deposited into Gene Expression Omnibus under <https://www.ncbi.nlm.nih.gov/geo/query/acc.cgi?acc=GSE142801>. Please

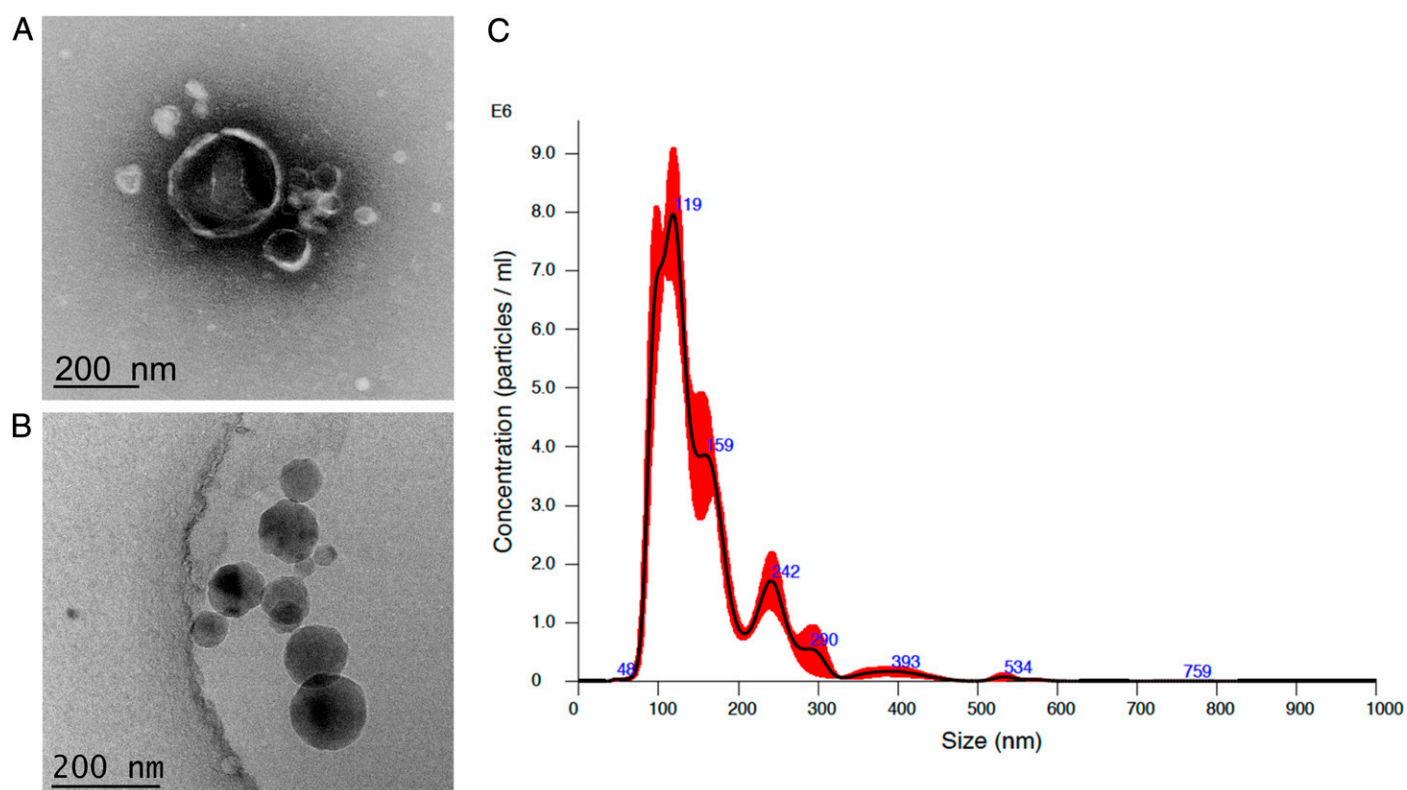


FIGURE 1. Characterization of EVs from *P. aeruginosa*.

EVs from *P. aeruginosa* were isolated as described in *Materials and Methods*. For visualization, EVs were negatively stained for TEM (A) or flash frozen for cryo-electron microscopy (B). NTA via NanoSight NS300 was used for EV particle counting and sizing (C).

TABLE I. 26 Proteins identified by MS from *P. aeruginosa* EVs

Protein	Accession Number	Molecular Mass (kDa)	Gene	Protein Compartmental Location
Elastase	P14756 ELAS_PSEAE	54	<i>lasB</i>	Extracellular
B-type flagellin	P72151 FLICB_PSEAE	49	<i>fliC</i>	Extracellular
Chitin-binding protein	Q91589 CBPD_PSEAE	42	<i>cbpD</i>	Extracellular
Outer membrane porin	P13794 PORF_PSEAE	38	<i>oprF</i>	Outer membrane vesicle
PhoP/Q outer membrane protein H1	G3XD11 G3XD11_PSEAE	22	<i>oprH</i>	Outer membrane vesicle
Protease Las A	P14789 LASA_PSEAE	46	<i>lasA</i>	Extracellular
Elongation factor Tu	P09591 EFTU_PSEAE	43	<i>tufA</i>	Cytosol
FigM	Q9HYP5 Q9HYP5_PSEAE	11	<i>flgM</i>	
Lipid A deacylase	Q9HVD1 PAGL_PSEAE	18	<i>pagL</i>	Outer membrane vesicle
Thioredoxin	Q9X2T1 THIO_PSEAE	12	<i>trxA</i>	Cytosol
Osmotically inducible lipoprotein OsmE	Q9HUT7 Q9HUT7_PSEAE	13	<i>osmE</i>	Outer membrane
Uncharacterized protein	Q9HWS1 Q9HWS1_PSEAE	16	<i>PA4107</i>	
Uncharacterized protein	Q9HZG8 Q9HZG8_PSEAE	12	<i>PA3040</i>	
Chaperone protein DnaK	Q9HV43 DNAK_PSEAE	68	<i>dnaK</i>	Cytosol
Arginine/ornithine binding protein	G3XD47 G3XD47_PSEAE	28	<i>aotJ</i>	Extracellular
B-type flagellar hook-associated protein	Q9K3C5 FLID2_PSEAE	49	<i>fliD</i>	Extracellular
Probable peroxidase	Q9HY81 Q9HY81_PSEAE	22	<i>PA3529</i>	
DNA-binding protein HU	P05384 DBHB_PSEAE	9	<i>hupB</i>	Cytosol
Usp domain-containing protein	Q9HYT5 Q9HYT5_PSEAE	16	<i>PA3309</i>	Outer membrane vesicle
OmpA-like domain-containing protein	Q915A7 Q915A7_PSEAE	25	<i>PA0833</i>	
Lysyl endopeptidase	Q9HWK6 LYSC_PSEAE	48	<i>prpL</i>	Extracellular
Uncharacterized protein	Q914N7 Q914N7_PSEAE	13	<i>PA1093</i>	
Uncharacterized protein	Q91384 Q91384_PSEAE	10	<i>PA1641</i>	
4-hydroxyphenylpyruvate dioxygenase	Q91576 HPPD_PSEAE	40	<i>hpd</i>	
Alkyl hydroperoxide reductase C	Q916Z3 Q916Z3_PSEAE	21	<i>ahpC</i>	Cytosol
Probable cold-shock protein	Q914H8 Q914H8_PSEAE	8	<i>PA1159</i>	Cytosol

contact corresponding author D.A.A. (David.A.Armstrong@hitchcock.org) for a token to access these data.

Statistical analysis

All gene expression data were presented as means \pm SD. GraphPad Prism (v7.0) analysis was used for paired sample *t* tests. Differential gene expression analysis of NanoString data was conducted using *edgeR* (v3.26.8) and *limma* (v3.40.6) packages in R (v3.6.1) (42, 43). The normalized data from NanoString were scaled to counts per million. Five hundred and forty-one genes with >10 cpm in at least two samples were used for downstream analysis. Likelihood ratio tests were conducted after fitting the gene expression data to a negative binomial generalized linear model. Three hundred and ten genes were determined as differentially expressed based on its likelihood ratio test false discovery rate value threshold of 0.05.

RESULTS

Characterization of EVs

Negative stain TEM was used to visualize isolated *P. aeruginosa* EVs (Fig. 1A). EVs were heterogeneous in size with a range of 30–600 nm in diameter. EVs show characteristic concave appearance common in negative staining. Additionally, cryo-electron microscopy was used to further visually confirm EV size range (Fig. 1B), and NTA was used for particle counting, sizing, and visualization. Several batches of *P. aeruginosa* EVs were isolated and used over the course of the study. A representative particle trace curve

from one batch of *P. aeruginosa* EVs analyzed via the NanoSight NS300 nanoparticle tracking instrument is shown in Fig. 1C. Mean particle diameter was 191.6 nm (\pm 94.4). Typical EV particle yield from a starting volume of 35 ml of *P. aeruginosa*-conditioned

TABLE II. Top 20 cytokines/chemokines altered in lung macrophages with *P. aeruginosa* EV treatment

Gene	Normalized Read Counts (\pm SD) ^a	
	Untreated	EV Treated (48 h)
<i>IL-1α</i>	170 (80)	3,661 (960)
<i>IL-1β</i>	370 (248)	27,130 (11,310)
<i>IL-6</i>	3.3 (4.3)	1,810 (1,230)
<i>IL-8</i>	1,502 (1,793)	102,843 (43,186)
<i>IL-10</i>	1.6 (0.6)	69 (44)
<i>IL-19</i>	1.0 (0.1)	679 (386)
<i>TGF-β1</i>	338 (33)	388 (74)
<i>TNF</i>	37 (21)	357 (153)
<i>CCL2 (MCP-1)</i>	48 (29)	3,861 (1,882)
<i>CCL3 (MIP-1α)</i>	3,653 (452)	10,822 (6,354)
<i>CCL4 (MIP-1β)</i>	183 (246)	4,136 (2,493)
<i>CCL7 (MCP-3)</i>	4.6 (4.2)	226.5 (144.3)
<i>CCL18 (MIP-4)</i>	14,051.3 (10,181.1)	5,355.1 (4,644.1)
<i>CCL20 (MIP-3α)</i>	152.8 (221.1)	8,081.9 (4,137.4)
<i>CCL23 (MIP-3)</i>	270.6 (195.8)	71.5 (34.2)
<i>CXCL1 (GROα)</i>	83.6 (138.9)	31,247.4 (18,633.5)
<i>CXCL2 (GROβ)</i>	146.0 (92.1)	5,344.8 (4,184.8)
<i>CXCL3 (GROγ)</i>	290.9 (276.0)	16,089.7 (8,477.7)
<i>CXCL5 (ENA-78)</i>	1,765.1 (2,118.8)	40,783.8 (6,306.1)
<i>CXCL16 (SRPSOX)</i>	1,325.7 (1,792.7)	2,589.1 (541.1)

n = 7 subjects.

^aNanoString PanCancer/Immunology gene expression assay.

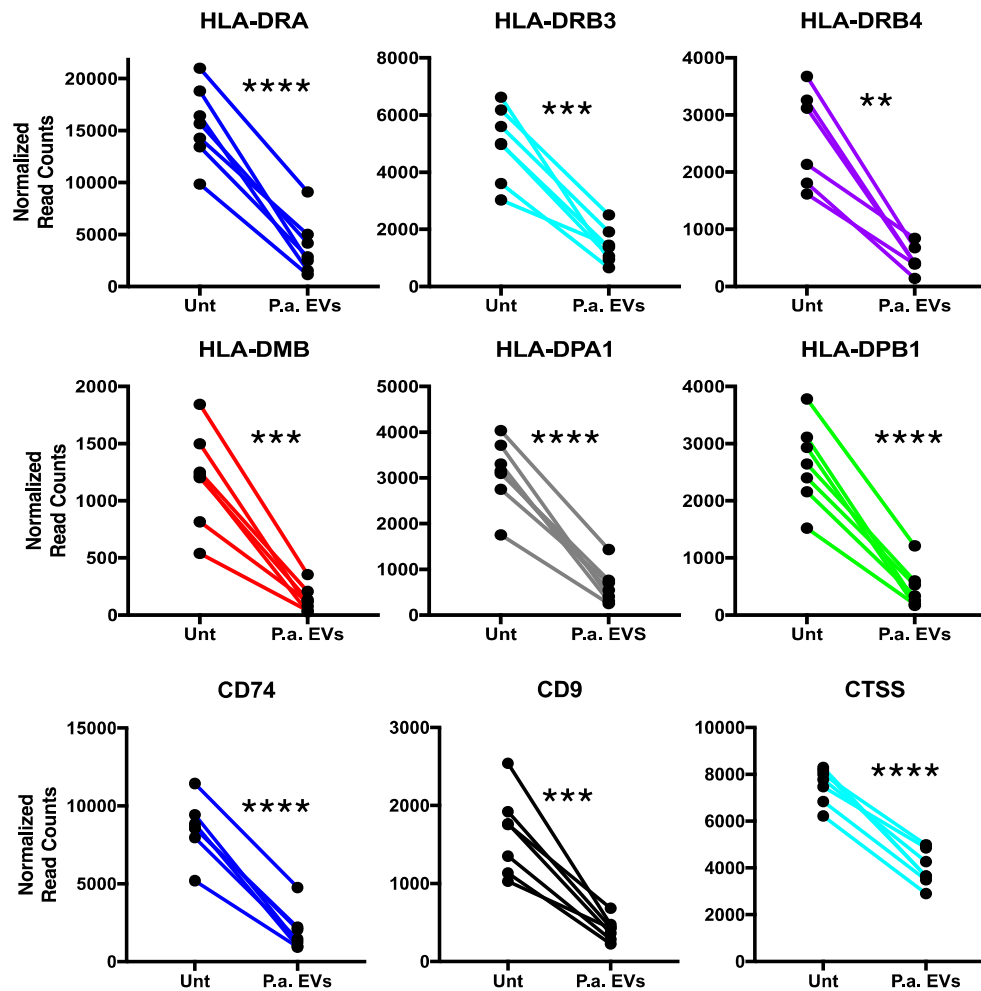


FIGURE 2. MHC class II– and class II–related gene expression is suppressed in lung macrophages following *P. aeruginosa* EV treatment.

HLA class II subunits *-DRA* and *-DRB*, along with paralogues *-DP* and enzyme *-DM* show decreased gene expression in all subjects ($n = 7$). Additionally, gene expression is suppressed for class II–related molecules *CD74*, *CD9*, and *cathepsin L*, 48 h after EV treatment in lung macrophages. ** $p < 0.01$, *** $p < 0.001$, **** $p < 0.0001$.

media was 4.25×10^9 total particles, corresponding to 1.2×10^8 particles/ml of media. A representative video of the *P. aeruginosa* EV particles passing through the 488-nm laser light of the NanoSight NS300 instrument is presented in the supplemental files as Supplemental Video 1.

A proteomics analysis was used to further characterize the *P. aeruginosa* EVs used in this study. MS was performed by MS (Bio-Works, Ann Arbor, MI). A total of 26 proteins were detected by MS, including numerous outer membrane proteins such as elastase, LasA, OmpF, OmpH, OsmE, PagL, and PA3309, as well as extracellular and cytosolic *P. aeruginosa* proteins. A complete list of the proteins identified, their accession numbers, associated genes, and compartmental locations are shown in Table I.

Cytokine/chemokine and MHC gene expression

Gene expression of numerous cytokines and chemokines were altered in lung macrophages following 48-h treatment with

P. aeruginosa EVs (Table II). A number of proinflammatory molecules such as IL-1 β , IL-8, and CXCL1 were notably higher, whereas two anti-inflammatory genes IL-6 and IL-10 were also higher. CCL18 and CCL23 and T and B cell chemoattractants were conspicuously lower.

Interestingly, *P. aeruginosa* EVs had a considerable suppressive effect on major histocompatibility molecule gene expression. Multiple MHC class II genes, in all subjects, were downregulated after 48 h of *P. aeruginosa* EV treatment (Fig. 2), including *HLA-DRA*, *HLA-DPA1*, *HLA-DPB1* ($p < 0.0001$), *HLA-DRB3*, *HLA-DMB* ($p < 0.001$), and *HLA-DRB4* ($p < 0.01$). Additionally, gene expression of MHC class II–related molecules *CD74* (HLA-DR Ag–associated invariant chain), *cathepsin S (CTSS)* ($p < 0.0001$) and *CD9* (tetraspanin-29) ($p < 0.001$) were suppressed following 48-h *P. aeruginosa* EV treatment. Furthermore, two MHC class I molecules, *HLA-A* and *HLA-B* ($p < 0.001$), were suppressed as well under our infection model experimental conditions (Supplemental Fig. 1). A full list of the 310 differentially expressed

TABLE III. Gene expression changes in lung macrophages with *P. aeruginosa* EV treatment versus LPS only

Gene	Normalized Read Counts ^a			
	<i>P. aeruginosa</i> EVs		LPS Only	
	Untreated	EV Treated	Untreated	LPS Treated
<i>CCL3</i>	362	10,822	262	11,336
<i>CCL3L1</i>	436	13,778	238	15,346
<i>CCL4</i>	183	4,136	81	4,608
<i>CCL18</i>	14,051	5,355	6,762	3,409
<i>CD14</i>	788	7,891	720	6,187
<i>CD44</i>	2,426	5,581	3,444	5,774
<i>CD74</i>	8,574	1,947	6,127	1,240
<i>CD81</i>	6,882	3,512	6,359	3,368
<i>CTSS</i>	7,537	3,974	6,103	3,260
<i>CXCL2</i>	146	5,345	60	3,764
<i>CXCL3</i>	291	16,090	74	13,847
<i>CXCL5</i>	1,765	40,784	708	39,122
<i>HLA-A</i>	4,564	2,287	3,204	2,086
<i>HLA-B</i>	4,015	2,351	4,153	2,823
<i>HLA-DRA</i>	15,646	3,758	11,216	2,430
<i>HLA-DRB3</i>	5,002	1,413	3,820	925
<i>IL-1β</i>	370	27,129	176	22,714
<i>IL-1RN</i>	229	1,086	463	2,502
<i>IL-8</i>	1,502	102,843	766	67,858
<i>LAMP1</i>	2,631	1,727	3,707	2,095
<i>LGALS3</i>	5,035	1,840	4,480	1,890
<i>MARCO</i>	1,912	652	880	152
<i>MRC1</i>	1,046	1,652	669	2,276
<i>S100A8</i>	407	2,492	342	2,638
<i>SH2D1B</i>	765	18,478	347	17,515

n = 2.

^a*P. aeruginosa*-derived LPS (1,000 ng/ml) 48 h.

genes following 48-h *P. aeruginosa* EV treatment is presented in Supplemental Table I.

To examine the potential contribution of LPS alone, which is contained on the surface of EVs, we conducted additional experiments using *Pseudomonas*-derived LPS in vitro. Interestingly, the effects of *P. aeruginosa* EVs on lung macrophages noted above were very similar to those effects seen in in vitro experiments with *Pseudomonas*-derived LPS alone shown in Table III. Alterations of cytokine/chemokine gene expression as well as decreases of MHC-related molecules occurred with 48-h LPS treatment (1000 ng/ml), indicating that LPS contained either on or within *P. aeruginosa* EVs was responsible for much, if not all, of these gene expression changes, therefore establishing the relevance of testing an infection model with EVs as a diffusible virulence agent.

MHC-related protein levels in lung macrophages

As an independent validation of the gene expression results, we next measured protein levels in lung macrophages untreated or exposed to *P. aeruginosa* EVs for 24 and 48 h. Lung macrophages from an additional four subjects were used in this portion of the study with representative results presented in Fig. 3. Total cellular protein of CD74 and CD9 were partially reduced at 24 h of EV treatment and further reduced at the 48-h time point. The MHC molecule HLA-DRA was increased at 24 h but modestly decreased

by 48 h. However, it is not particularly surprising to observe only modest decreases in MHC-DRA and -DRB proteins at 48 h given their half-lives of 20–50 h on human cells (44, 45) and that others have noted cell surface stabilization of MHC molecules with TLR ligand engagement (46). As additional confirmation, we show both gene expression and protein analysis for CD14, a molecule that was significantly upregulated in our infection model (Supplemental Fig. 2).

To explore the possible cellular mechanism of widespread reduction of MHC-related molecules in our infection model, we leveraged genome-wide DNA methylation data from the Illumina EPIC DNA methylation array and focused on regulatory regions associated with MHC molecules. *P. aeruginosa* EVs result in altered DNA methylation in lung macrophage MHC genes. We observed significant hypomethylation associated with *P. aeruginosa* EV treatment at three CpG sites in exon 8 of complement factor B (*CFB*) gene, an MHC class III gene. *CFB* gene body hypomethylation related with *P. aeruginosa* EV treatment ranged from 5.1 to 18.8% (Table IV). These differentially methylated CpGs in the gene body of *CFB* are situated between MHC class I and II regions (Supplemental Fig. 3). We next tested the correlation between their methylation level and expression of MHC genes. We observed a strong correlation between DNA methylation of the *CFB* gene body CpGs and gene expression of both *HLA-DRA* (Fig. 4A–C) and *HLA-DRB3* (Fig. 4D–F). A detailed correlation matrix heatmap of all *CFB* CpGs on the EPIC array and all MHC genes on

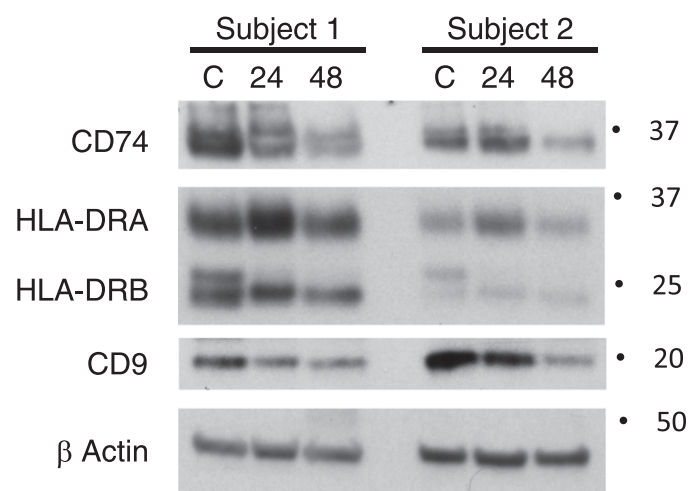


FIGURE 3. Protein levels of MHC-related molecules decrease in lung macrophages exposed to *P. aeruginosa* EVs for up to 48 h.

MHC class II-related proteins CD74 and CD9 decrease after 48 h but show some variability at the 24 h time point. HLA-DR subunits were modestly diminished at 48 h after *P. aeruginosa* EV treatment. TLR engagement has been reported to partly stabilize HLA-DR surface molecules, potentially leading to a modest depletion at the protein level. A complement of four additional subjects were used for cellular protein studies (see *Materials and Methods*). Responses were similar in three of four subjects.

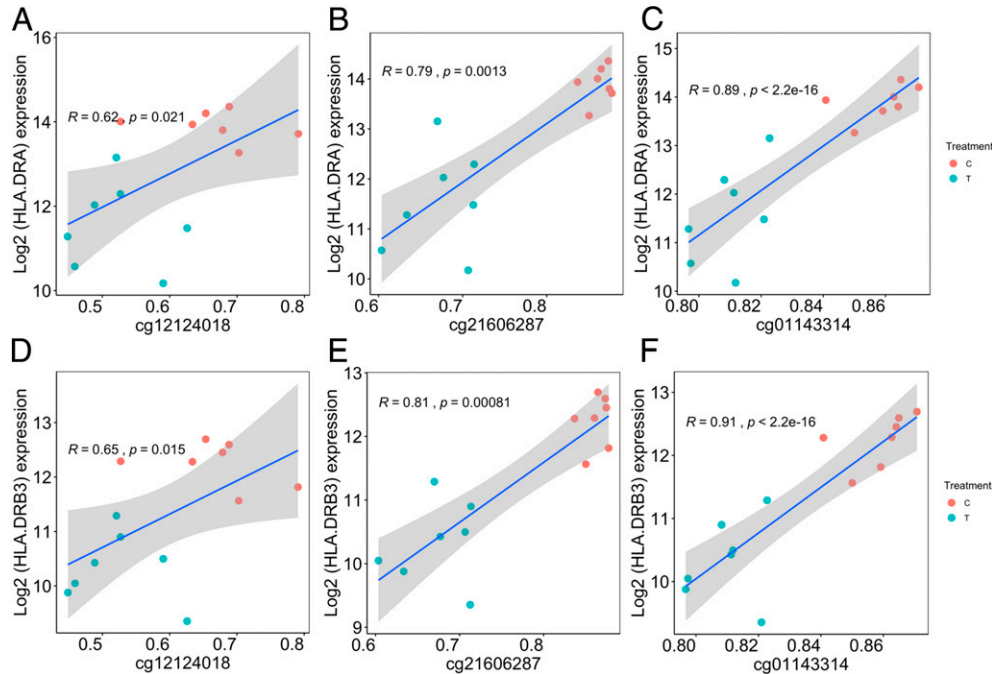


FIGURE 4. CFB Exon 8 CpGs methylation shows strong correlation to HLA-DRA and HLA-DRB3 gene expression.

Correlation coefficients and linear regression p values were determined for CpGs in exon 8 (cg12124018, cg21606287, and cg01143314) associated with gene expression of HLA-DRA (A–C) and HLA-DRB3 (D–F). Correlations were calculated using the Spearman rank correlation method. Linear regression lines and its 95% confidence intervals is indicated by the blue lines and gray bands, respectively.

the NanoString Cancer/Immune gene expression panel is shown in Fig. 5, with the exon 8 containing CpGs highlighted.

DISCUSSION

The goal of this study was to determine if EVs, lipid bilayer vesicles secreted from *P. aeruginosa*, could alter lung macrophage gene expression, specifically at MHC genes associated with Ag presentation and pathogen clearance. We have used human lung macrophages and *P. aeruginosa* EVs as an in vitro model for lung infection, simulating how microbial EVs may diffuse some distance from their cell of origin, potentially affecting innate immune cells not in direct physical contact with individual microbes at sites of bacterial colonization in the lung. Our results demonstrate that when macrophages are exposed to *P. aeruginosa* EVs, MHC-related genes and protein levels are suppressed. Additionally, we observed hypomethylation of a DNA regulatory region situated directly between MHC class I and class II genes within *CFB* gene body. Hypomethylation of three closely situated CpGs within the *CFB* gene showed strong correlation with decreased MHC gene expression, hence the potential driving mechanism of MHC class II mRNA suppression.

In CF, lung macrophages have been shown to exhibit decreased phagocytosis and defective bacterial clearance (21, 22, 47). This phenotype is likely influenced by both intrinsic (i.e., CFTR expression) (48) and extrinsic factors (i.e., polymicrobial

environment) (49, 50). A number of recent studies have examined how virulence and other pathogen-derived factors as well as whole EVs can affect host cells in a pathogen–host interaction. Milillo et al. (51) showed that RNA from *Brucella abortus* contributes to inhibit MHC class II–restricted Ag presentation in macrophages. Additionally, Bomberger et al. (10) showed that *P. aeruginosa* virulence factor Cif inhibits TAP function and MHC class I Ag presentation in epithelial cells. Also, Park et al. (52) were one of the first studies to show that outer membrane vesicles or EVs from *P. aeruginosa* could cause pulmonary inflammation in vivo in the absence of whole bacteria. Finally, Cecil et al. (38) demonstrated that EVs from oral pathogens *P. gingivalis*, *Treponema denticola*, and *Tannerella forsythia* have significant immunomodulatory effects on monocytes and macrophages.

In this report, we demonstrate for the first time, to our knowledge, that EVs from a common CF pathogen, *P. aeruginosa*, suppress expression of MHC-related molecules in human lung macrophages. Nine different MHC class II–related genes/molecules including *HLA-DRA*, *-DRBs*, *-DMB*, and *-DPs* (chromosome 6); *CD74* (chr5); *CD9* (chr1); and *CTSS* (chr12) are diminished with *P. aeruginosa* EV exposure. HLA-DRA and -DRB are the heterodimeric subunits of the MHC II complex that bind processed antigenic fragments within the phagolysosome (27). HLA-DMB is the enzyme that removes CLIP from the HLA-DR cleft so that the antigenic fragments can bind (27). HLA-DP are class II β -chain paralogues. CD74, also called Ii, is the class II invariant chain that initially blocks the MHC II cleft in the

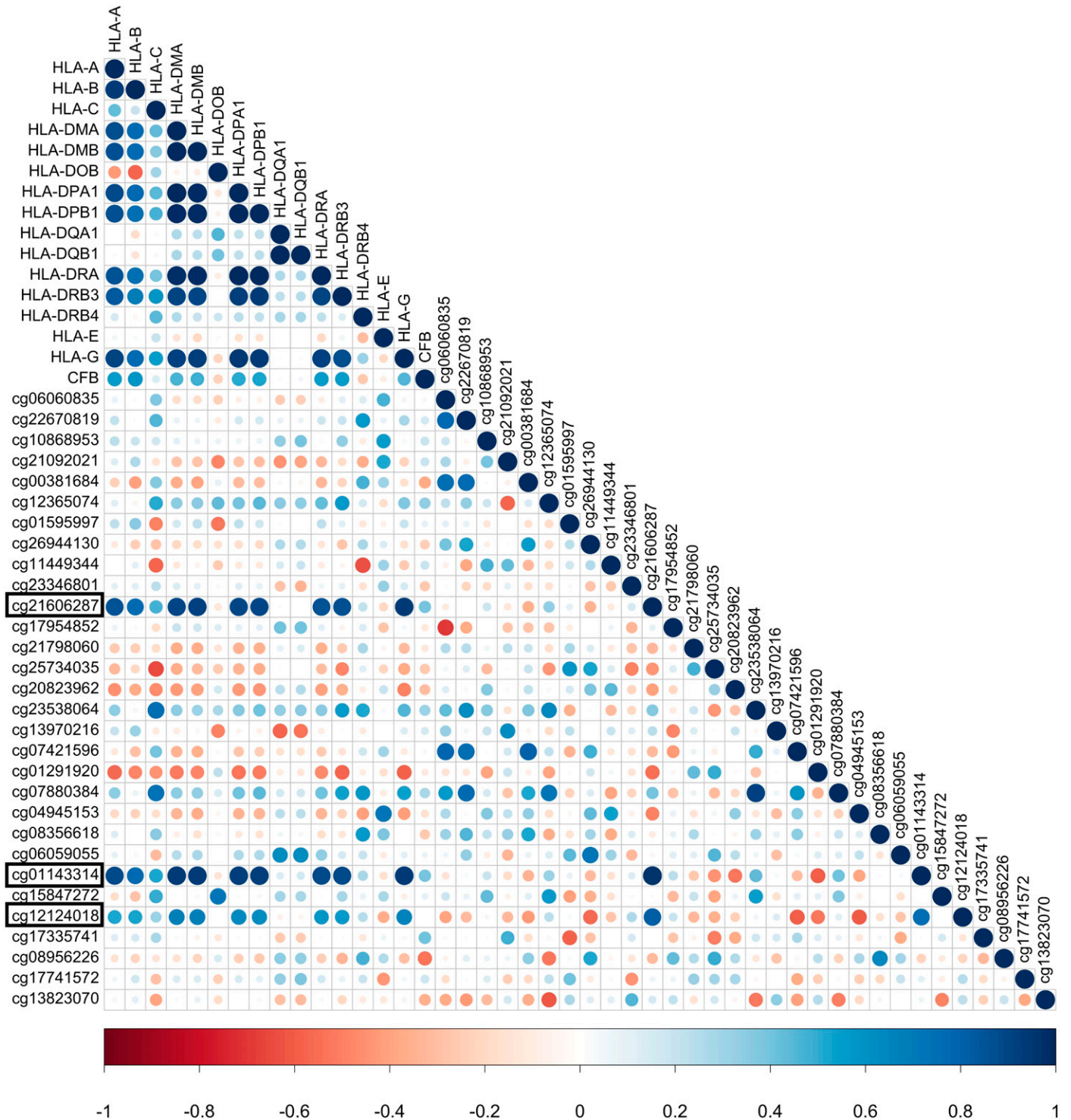


FIGURE 5. Correlation plot of CFB-associated CpG methylation and MHC-related gene expression.

Strong correlation ($R > 0.55$, Spearman rank correlation method) exists between methylation of CFB CpGs (cg21606287, cg01143314, and cg12124018) and gene expression of multiple MHC-related genes. Hypomethylated CFB CpGs in exon 8 are highlighted in black rectangles. Size of the circles indicates the absolute value of corresponding correlation coefficients. Color indicates the direction of correlation from strong negative correlation (dark red, correlation coefficient = -1) to strong positive correlation (dark blue, correlation coefficient = 1).

TABLE IV. Chromosomal location of HLA genes and CFB hypomethylated CpGs

Gene Name/EPIC cg ID	Class	Gene/CpG Location	Hypomethylation Change (%)
<i>HLA-A</i>	I	chr6: 29,881,755–30,002,076	
<i>HLA-B</i>	I	chr6: 31,259,328–31,347,305	
<i>CFB</i>	III	chr6: 31,945,650–31,952,084	
<i>CFB</i> (cg12124018)	III	chr6: 31,948,906	–15.8
<i>CFB</i> (cg21606287)	III	chr6: 31,948,928	–18.8
<i>CFB</i> (cg01143314)	III	chr6: 31,948,934	–5.1
<i>HLA-DRA</i>	II	chr6: 32,414,554–32,419,764	
<i>HLA-DRB3</i>	II	chr6: 32,449,765–32,462,852	
<i>HLA-DMB</i>	II	chr6: 33,025,327–33,043,825	

Ag-processing compartment or phagolysosome (27). CD9 regulates MHC II trafficking within the cell (53). CTSS is cathepsin S, a lysosomal cysteine protease that degrades CD74 and pathogen peptides within the phagolysosome (27). All of these molecules are intimately involved in MHC class II Ag processing and presentation to CD4⁺ T cells as a bridge between innate and adaptive immunity during a pathogen infection.

Additionally, we asked if the MHC-related effects seen may be attributed to LPS alone or some other yet-to-be-identified virulence factor within EVs. Interestingly, experiments with LPS alone demonstrated that LPS itself was responsible for much, if not all, of these gene expression changes in lung macrophages in our infection model.

The response we are observing has some of the hallmarks of endotoxin tolerance, however, other aspects, specifically IL-1 β and MHC molecules, are not consistent with tolerance. Studies on the mechanism of endotoxin tolerance have long history but are still in constant progress. However, the exact mechanism of endotoxin tolerance is still elusive, and many questions remain to be answered (54). In our infection model, it may be that human lung macrophages contain cell-specific subsets of tolerizeable genes and nontolerizeable genes with different behaviors after endotoxin stimulation. What we are observing may be a combination of an active host response (i.e., endotoxin tolerance) and an active pathogen-derived process to circumvent the host's immune response. Future studies should be directed toward answering this question.

Furthermore, we have identified, via genome-wide DNA methylation analysis, three specific CpGs on chromosome 6 within the *CFB* gene situated directly between MHC class I and MHC class II regions that may serve as a DNA regulatory region for MHC molecule gene expression. The CpGs of *CFB* are located ~500 kb from the class II *HLA-DRA* gene and 700 kb from the class I *HLA-B* gene. Hypomethylation (range 5.1–18.8%) of these CpG sites is strongly correlated with gene expression of multiple MHC genes.

Over 200 MHC molecules are clustered in a 3-MB region of chromosome 6 in humans. Multiple DNA regulatory regions (i.e., enhancers, silencers, and DHS regions) may be involved in MHC molecule coregulation (55). One type of regulatory element, enhancers, do not always act upon the closest gene promoter but can bypass neighboring genes to regulate genes located more distantly along a chromosome (56). And in some cases, individual

enhancers have been found to regulate multiple genes (57). One of the most extreme examples is the location of a DNA regulatory element, in this case an enhancer, is located 1 Mb upstream from the Sonic Hedgehog (*SHH*) gene, within an intron of the unrelated *LMBRI* gene (58, 59). We believe *CFB* gene methylation could be another example of a distal DNA regulatory element located in a neighboring gene (gene A; i.e., *CFB*), in which hypomethylation in the gene *CFB* results in transcriptional repression of gene B (i.e., MHC genes).

In addition to the MHC genes on chromosome 6, other MHC-related genes, such as *CTSS* and *CD74*, are located on alternate chromosomes (chromosomes 1 and 5, respectively). This suggests that *P. aeruginosa* EVs possess some factor(s) that specifically target MHC molecule suppression regardless of their chromosomal location as an immune evasion strategy. The exact mechanism of gene regulation across multiple differing chromosomes remains to be determined and should be the focus of future investigations.

This study has a number of strengths; however, this work also has a number of limitations. We cannot rule out that virulence factors or other yet-unidentified molecules within *P. aeruginosa* EVs beyond LPS may be contributing to the effects we are seeing in our infection model. Additionally, it is not currently known if the response seen is an active host response (i.e., tolerance), an operative pathogen process to circumvent host defenses or some combination of both.

In conclusion, in our infection model, we have demonstrated the immunosuppressive potential of *P. aeruginosa* EVs on lung macrophages. These effects appear to be largely attributable to LPS contained on or within EVs and may be contingent upon the diffusible nature of EVs. In the polymicrobial community of a CF lung infection, the local milieu is significantly more complicated than presented in our model, but based on the observations demonstrated in this study, we suggest that the downregulation of MHC molecules by *P. aeruginosa* EVs may be contributing, along with other extrinsic factors from *P. aeruginosa* and additional pathogens, to decreased Ag presentation and pathogen clearance in lung infection.

DISCLOSURES

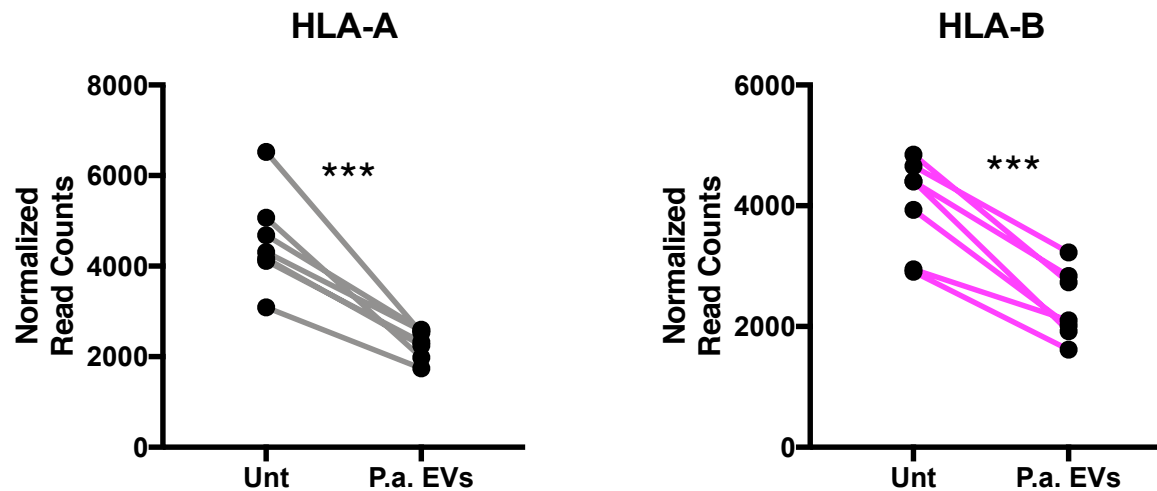
The authors have no financial conflicts of interest.

REFERENCES

- O'Sullivan, B. P., and S. D. Freedman. 2009. Cystic fibrosis. *Lancet* 373: 1891–1904.
- Cystic Fibrosis Foundation. 2018. *Cystic Fibrosis Foundation Patient Registry 2017 Annual Data Report*. Cystic Fibrosis Foundation, Bethesda, MD.
- Elborn, J. S., and D. J. Shale. 1990. Cystic fibrosis. 2. Lung injury in cystic fibrosis. *Thorax* 45: 970–973.
- Elborn, J. S. 2016. Cystic fibrosis. *Lancet* 388: 2519–2531.
- Gilligan, P. H. 1991. Microbiology of airway disease in patients with cystic fibrosis. *Clin. Microbiol. Rev.* 4: 35–51.
- Malhotra, S., D. Hayes, Jr., and D. J. Wozniak. 2019. Cystic fibrosis and *Pseudomonas aeruginosa*: the host-microbe interface. *Clin. Microbiol. Rev.* 32: e00138-18.
- Briard, B., G. L. A. Mislin, J. P. Latgé, and A. Beauvais. 2019. Interactions between *Aspergillus fumigatus* and pulmonary bacteria: current state of the field, new data, and future perspective. *J. Fungi (Basel)* 5: 48.
- Chmiel, J. F., T. R. Aksmit, S. H. Chotirmall, E. C. Dasenbrook, J. S. Elborn, J. J. LiPuma, S. C. Ranganathan, V. J. Waters, and F. A. Ratjen. 2014. Antibiotic management of lung infections in cystic fibrosis. II. Nontuberculous mycobacteria, anaerobic bacteria, and fungi. *Ann. Am. Thorac. Soc.* 11: 1298–1306.
- Koeppen, K., R. Barnaby, A. A. Jackson, S. A. Gerber, D. A. Hogan, and B. A. Stanton. 2019. Tobramycin reduces key virulence determinants in the proteome of *Pseudomonas aeruginosa* outer membrane vesicles. *PLoS One* 14: e0211290.
- Bomberger, J. M., K. H. Ely, N. Bangia, S. Ye, K. A. Green, W. R. Green, R. I. Enelow, and B. A. Stanton. 2014. *Pseudomonas aeruginosa* Cif protein enhances the ubiquitination and proteasomal degradation of the transporter associated with antigen processing (TAP) and reduces major histocompatibility complex (MHC) class I antigen presentation. *J. Biol. Chem.* 289: 152–162.
- Bomberger, J. M., D. P. Maceachran, B. A. Coutermarsh, S. Ye, G. A. O'Toole, and B. A. Stanton. 2009. Long-distance delivery of bacterial virulence factors by *Pseudomonas aeruginosa* outer membrane vesicles. *PLoS Pathog.* 5: e1000382.
- Ellis, T. N., and M. J. Kuehn. 2010. Virulence and immunomodulatory roles of bacterial outer membrane vesicles. *Microbiol. Mol. Biol. Rev.* 74: 81–94.
- Koeppen, K., T. H. Hampton, M. Jarek, M. Scharfe, S. A. Gerber, D. W. Mielcarz, E. G. Demers, E. L. Dolben, J. H. Hammond, D. A. Hogan, and B. A. Stanton. 2016. A novel mechanism of host-pathogen interaction through sRNA in bacterial outer membrane vesicles. *PLoS Pathog.* 12: e1005672.
- Renelli, M., V. Matias, R. Y. Lo, and T. J. Beveridge. 2004. DNA-containing membrane vesicles of *Pseudomonas aeruginosa* PAO1 and their genetic transformation potential. *Microbiology* 150: 2161–2169.
- Buzas, E. I., B. György, G. Nagy, A. Falus, and S. Gay. 2014. Emerging role of extracellular vesicles in inflammatory diseases. *Nat. Rev. Rheumatol.* 10: 356–364.
- Liu, S., A. P. da Cunha, R. M. Rezende, R. Cialic, Z. Wei, L. Bry, L. E. Comstock, R. Gandhi, and H. L. Weiner. 2016. The host shapes the gut microbiota via fecal microRNA. *Cell Host Microbe* 19: 32–43.
- Properzi, F., M. Logozzi, and S. Fais. 2013. Exosomes: the future of biomarkers in medicine. *Biomarkers Med.* 7: 769–778.
- Tsatsaronis, J. A., S. Franch-Arroyo, U. Resch, and E. Charpentier. 2018. Extracellular vesicle RNA: a universal mediator of microbial communication? *Trends Microbiol.* 26: 401–410.
- Cecil, J. D., N. Sirisaengtaksin, N. M. O'Brien-Simpson, and A. M. Krachler. 2019. Outer membrane vesicle-host cell interactions. *Microbiol. Spectr.* DOI: 10.1128/microbiolspec.PSIB-0001-2018.
- Zhang, W., X. Jiang, J. Bao, Y. Wang, H. Liu, and L. Tang. 2018. Exosomes in pathogen infections: a bridge to deliver molecules and link functions. *Front. Immunol.* 9: 90.
- Bruscia, E. M., and T. L. Bonfield. 2016. Innate and adaptive immunity in cystic fibrosis. *Clin. Chest Med.* 37: 17–29.
- Bruscia, E. M., and T. L. Bonfield. 2016. Cystic fibrosis lung immunity: the role of the macrophage. *J. Innate Immun.* 8: 550–563.
- Xing, Z., S. Afkhami, J. Bavananthasivam, D. K. Fritz, M. R. D'Agostino, M. Vaseghi-Shanjani, Y. Yao, and M. Jeyanathan. 2020. Innate immune memory of tissue-resident macrophages and trained innate immunity: re-vamping vaccine concept and strategies. *J. Leukoc. Biol.* DOI: 10.1002/JLB.4MRO220-446R.
- Hirayama, D., T. Iida, and H. Nakase. 2017. The phagocytic function of macrophage-enforcing innate immunity and tissue homeostasis. *Int. J. Mol. Sci.* 19: 92.
- Rossi, G., A. Cavazza, P. Spagnolo, S. Bellafiore, E. Kuhn, P. Carassai, L. Caramanico, G. Montanari, G. Cappiello, A. Andreani, et al. 2017. The role of macrophages in interstitial lung diseases. *Eur. Respir. Rev.* 26: 170009.
- Malhotra, S., D. Hayes, Jr., and D. J. Wozniak. 2019. Mucoid *Pseudomonas aeruginosa* and regional inflammation in the cystic fibrosis lung. *J. Cyst. Fibros.* 18: 796–803.
- Roche, P. A., and K. Furuta. 2015. The ins and outs of MHC class II-mediated antigen processing and presentation. *Nat. Rev. Immunol.* 15: 203–216.
- Tortorella, D., B. E. Gewurz, M. H. Furman, D. J. Schust, and H. L. Ploegh. 2000. Viral subversion of the immune system. *Annu. Rev. Immunol.* 18: 861–926.
- Antonia, A. L., K. D. Gibbs, E. D. Trahair, K. J. Pittman, A. T. Martin, B. H. Schott, J. S. Smith, S. Rajagopal, J. W. Thompson, R. L. Reinhardt, and D. C. Ko. 2019. Pathogen evasion of chemokine response through suppression of CXCL10. *Front. Cell. Infect. Microbiol.* 9: 280.
- Srisatjaluk, R., G. J. Kotwal, L. A. Hunt, and D. E. Justus. 2002. Modulation of gamma interferon-induced major histocompatibility complex class II gene expression by *Porphyromonas gingivalis* membrane vesicles. *Infect. Immun.* 70: 1185–1192.
- Bessich, J. L., A. B. Nymon, L. A. Moulton, D. Dorman, and A. Ashare. 2013. Low levels of insulin-like growth factor-1 contribute to alveolar macrophage dysfunction in cystic fibrosis. *J. Immunol.* 191: 378–385.
- Chen, Y., D. A. Armstrong, L. A. Salas, H. F. Hazlett, A. B. Nymon, J. A. Dessaint, D. S. Aridgides, D. L. Mellinger, X. Liu, B. C. Christensen, and A. Ashare. 2018. Genome-wide DNA methylation profiling shows a distinct epigenetic signature associated with lung macrophages in cystic fibrosis. *Clin. Epigenetics* 10: 152.
- Jung, M. K., and J. Y. Mun. 2018. Sample preparation and imaging of exosomes by transmission electron microscopy. *J. Vis. Exp.* 131:56482.
- Oosthuyzen, W., N. E. Sime, J. R. Ivy, E. J. Turtle, J. M. Street, J. Pound, L. E. Bath, D. J. Webb, C. D. Gregory, M. A. Bailey, and J. W. Dear. 2013. Quantification of human urinary exosomes by nanoparticle tracking analysis. *J. Physiol.* 591: 5833–5842.
- Nemec, S. F., A. A. Bankier, and R. L. Eisenberg. 2013. Upper lobe-predominant diseases of the lung. *AJR Am. J. Roentgenol.* 200: W222–W237.
- Armstrong, D. A., Y. Chen, J. A. Dessaint, D. S. Aridgides, J. Y. Channon, D. L. Mellinger, B. C. Christensen, and A. Ashare. 2019. DNA methylation changes in regional lung macrophages are associated with metabolic differences. *Immunohorizons* 3: 274–281.
- Armstrong, D. A., A. B. Nymon, C. S. Ringelberg, C. Lesseur, H. F. Hazlett, L. Howard, C. J. Marsit, and A. Ashare. 2017. Pulmonary microRNA profiling: implications in upper lobe predominant lung disease. *Clin. Epigenetics* 9: 56.
- Cecil, J. D., N. M. O'Brien-Simpson, J. C. Lenzo, J. A. Holden, W. Singleton, A. Perez-Gonzalez, A. Mansell, and E. C. Reynolds. 2017. Outer membrane vesicles prime and activate macrophage

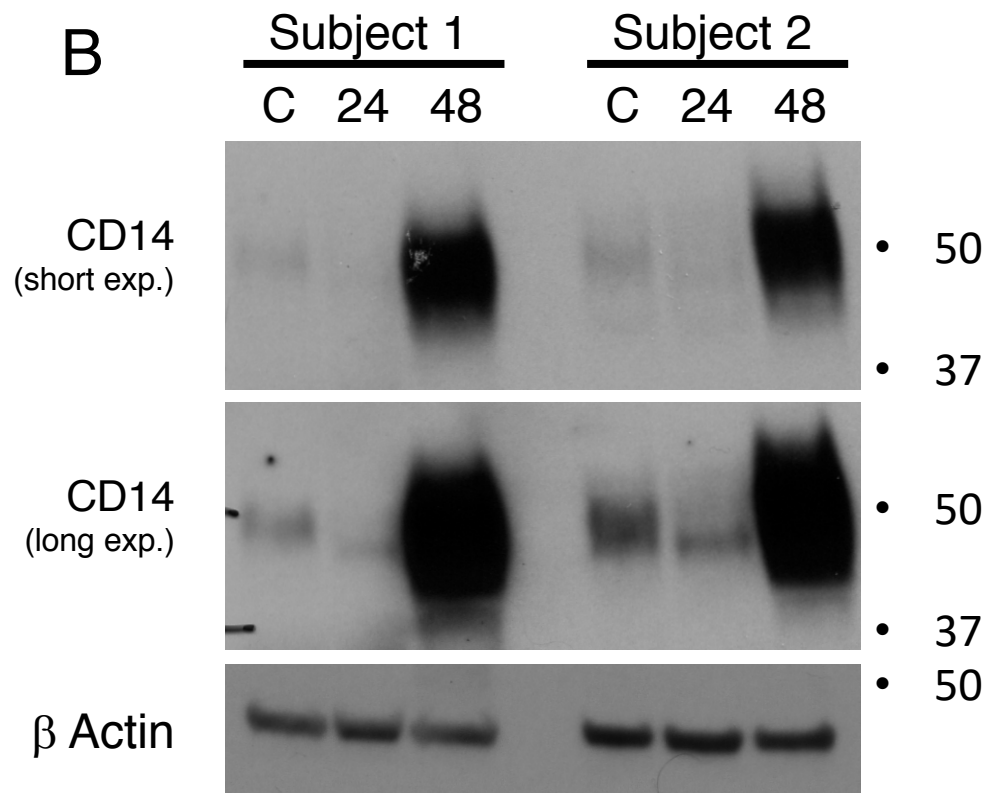
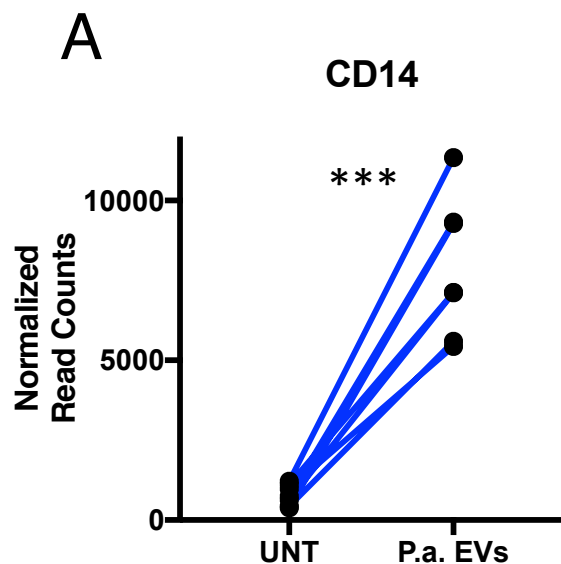
- inflammasomes and cytokine secretion *in vitro* and *in vivo*. *Front. Immunol.* 8: 1017.
39. Kling, T., A. Wenger, S. Beck, and H. Carén. 2017. Validation of the MethylationEPIC BeadChip for fresh-frozen and formalin-fixed paraffin-embedded tumours. *Clin. Epigenetics* 9: 33.
40. Aryee, M. J., A. E. Jaffe, H. Corrada-Bravo, C. Ladd-Acosta, A. P. Feinberg, K. D. Hansen, and R. A. Irizarry. 2014. Minfi: a flexible and comprehensive bioconductor package for the analysis of Infinium DNA methylation microarrays. *Bioinformatics* 30: 1363–1369.
41. Zhou, W., P. W. Laird, and H. Shen. 2017. Comprehensive characterization, annotation and innovative use of Infinium DNA methylation BeadChip probes. *Nucleic Acids Res.* 45: e22.
42. Ritchie, M. E., B. Phipson, D. Wu, Y. Hu, C. W. Law, W. Shi, and G. K. Smyth. 2015. Limma powers differential expression analyses for RNA-sequencing and microarray studies. *Nucleic Acids Res.* 43: e47.
43. Robinson, M. D., D. J. McCarthy, and G. K. Smyth. 2010. edgeR: a Bioconductor package for differential expression analysis of digital gene expression data. *Bioinformatics* 26: 139–140.
44. Lanzavecchia, A., P. A. Reid, and C. Watts. 1992. Irreversible association of peptides with class II MHC molecules in living cells. *Nature* 357: 249–252.
45. Müller, K. P., J. Schumacher, and B. A. Kyewski. 1993. Half-life of antigen/major histocompatibility complex class II complexes in vivo: intra- and interorgan variations. *Eur. J. Immunol.* 23: 3203–3207.
46. De Gassart, A., F. De Angelis Rigotti, and E. Gatti. 2013. MHC-II ubiquitination. *Methods Mol. Biol.* 960: 517–527.
47. Barnaby, R., K. Koepfen, A. Nymon, T. H. Hampton, B. Berwin, A. Ashare, and B. A. Stanton. 2018. Lumacaftor (VX-809) restores the ability of CF macrophages to phagocytose and kill *Pseudomonas aeruginosa*. *Am. J. Physiol. Lung Cell. Mol. Physiol.* 314: L432–L438.
48. Sorio, C., M. Buffelli, C. Angiari, M. Ettore, J. Johansson, M. Vezzalini, L. Viviani, M. Ricciardi, G. Verzè, B. M. Assael, and P. Melotti. 2011. Defective CFTR expression and function are detectable in blood monocytes: development of a new blood test for cystic fibrosis. *PLoS One* 6: e22212.
49. Baishya, J., and C. A. Wakeman. 2019. Selective pressures during chronic infection drive microbial competition and cooperation. *NPJ Biofilms Microbiomes* 5: 16.
50. Bruscia, E. M., P. X. Zhang, E. Ferreira, C. Caputo, J. W. Emerson, D. Tuck, D. S. Krause, and M. E. Egan. 2009. Macrophages directly contribute to the exaggerated inflammatory response in cystic fibrosis transmembrane conductance regulator^{-/-} mice. *Am. J. Respir. Cell Mol. Biol.* 40: 295–304.
51. Milillo, M. A., A. Trotta, A. Serafino, J. L. Marin Franco, F. V. Marinho, J. Alcaín, M. Genoula, L. Balboa, S. C. Oliveira, G. H. Giambartolomei, and P. Barrionuevo. 2019. Bacterial RNA contributes to the down-modulation of MHC-II expression on monocytes/macrophages diminishing CD4⁺ T cell responses. *Front. Immunol.* 10: 2181.
52. Park, K. S., J. Lee, S. C. Jang, S. R. Kim, M. H. Jang, J. Lötvall, Y. K. Kim, and Y. S. Gho. 2013. Pulmonary inflammation induced by bacteria-free outer membrane vesicles from *Pseudomonas aeruginosa*. *Am. J. Respir. Cell Mol. Biol.* 49: 637–645.
53. Rocha-Perugini, V., G. Martínez Del Hoyo, J. M. González-Granado, M. Ramírez-Huesca, V. Zorita, E. Rubinstein, C. Boucheix, and F. Sánchez-Madrid. 2017. CD9 regulates major histocompatibility complex class II trafficking in monocyte-derived dendritic cells. *Mol. Cell. Biol.* 37: e00202-17.
54. Liu, D., S. Cao, Y. Zhou, and Y. Xiong. 2019. Recent advances in endotoxin tolerance. *J. Cell. Biochem.* 120: 56–70.
55. Kolovos, P., T. A. Knoch, F. G. Grosveld, P. R. Cook, and A. Papantonis. 2012. Enhancers and silencers: an integrated and simple model for their function. *Epigenetics Chromatin* 5: 1.
56. Pennacchio, L. A., W. Bickmore, A. Dean, M. A. Nobrega, and G. Bejerano. 2013. Enhancers: five essential questions. *Nat. Rev. Genet.* 14: 288–295.
57. Mohrs, M., C. M. Blankespoor, Z. E. Wang, G. G. Loots, V. Afzal, H. Hadeiba, K. Shinkai, E. M. Rubin, and R. M. Locksley. 2001. Deletion of a coordinate regulator of type 2 cytokine expression in mice. *Nat. Immunol.* 2: 842–847.
58. Stadhouders, R., A. van den Heuvel, P. Kolovos, R. Jorna, K. Leslie, F. Grosveld, and E. Soler. 2012. Transcription regulation by distal enhancers: who's in the loop? *Transcription* 3: 181–186.
59. Sagai, T., M. Hosoya, Y. Mizushima, M. Tamura, and T. Shiroishi. 2005. Elimination of a long-range cis-regulatory module causes complete loss of limb-specific Shh expression and truncation of the mouse limb. *Development* 132: 797–803.

Supplemental Figure 1



Supplemental Fig 1. MHC Class I gene expression is suppressed in lung macrophages with 48 hour *P.a.* EV treatment. NanoString nCounter gene expression assay utilizing the cancer/immune panel of 770 genes was used to measure MHC Class I gene expression. *HLA-A* and *HLA-B* mRNA was diminished post EV-treatment. *** $P < 0.001$.

Supplemental Figure 2

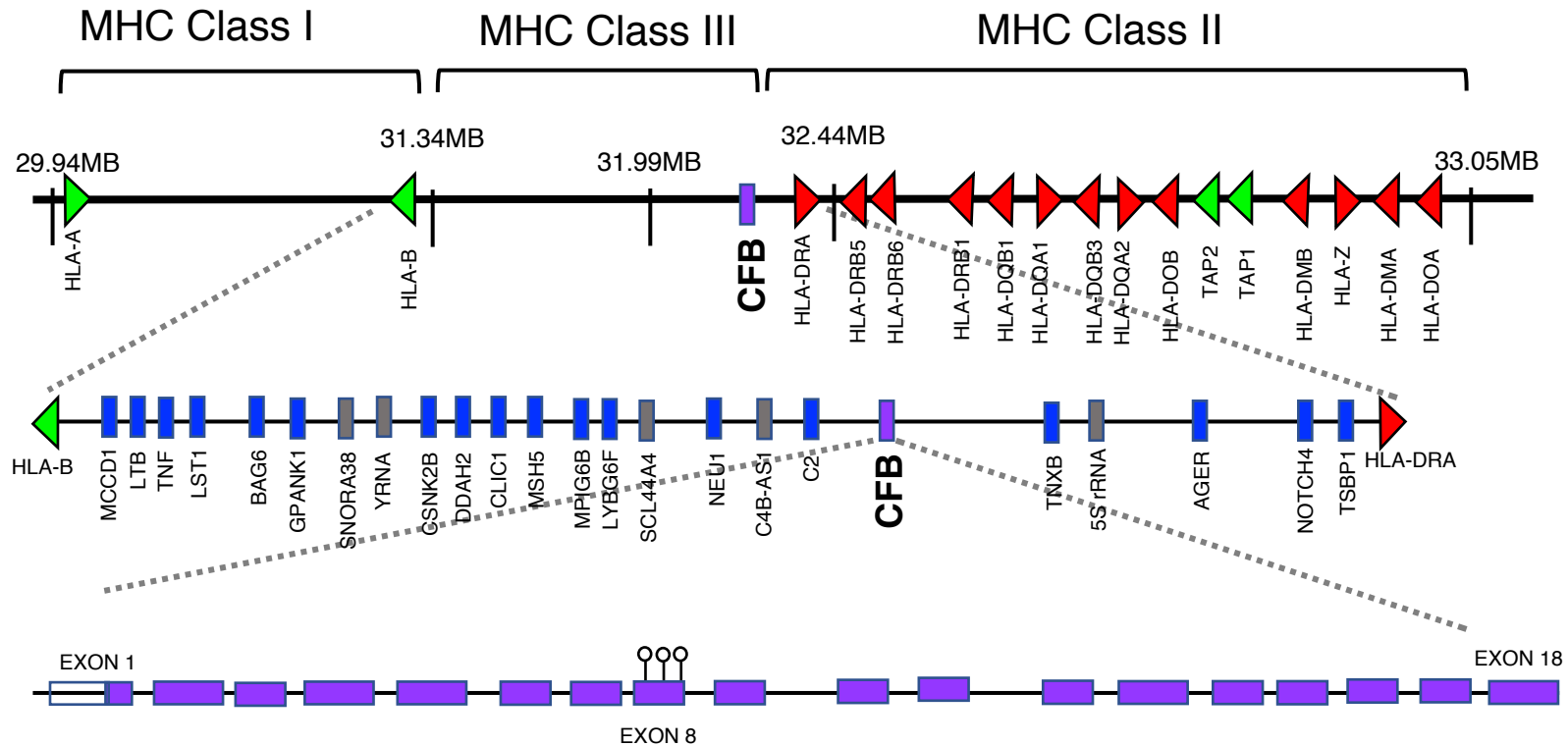


Supplemental Figure 2. Gene expression and protein expression on CD14 in lung macrophages increases with *P. aeruginosa* EV treatment.

CD14 gene expression in lung macrophages from all subjects (n=7) increases with P.a. EV-treatment (A). Protein expression increase at 48 hours confirms and validates mRNA measurement (B).***P < 0.001.

Supplemental Figure 3

Chromosome 6



Supplemental Figure 3. Schematic representation of MHC gene clustering on chromosome 6. MHC class I genes, in general are situated more toward 5' end of chromosome 6 segment and class II genes situated more 3' on chromosome 6. *Complement factor B (CFB)*, one of approximately 60 MHC class III genes is situated directly in between class I & II. Schematic shows examples of genes contained in this MHC class III region of chromosome 6 (not all inclusive or to exact scale). *CFB* contains 18 exons. The three CpGs identified as significantly hypomethylated are located in exon 8 of the *CFB* gene.

Supplemental Video 1

Nanoparticle tracking analysis (NTA) of *P. aeruginosa* extracellular vesicles (EVs).

P. aeruginosa extracellular vesicles were measured by NTA. EVs were isolated via affinity resin, diluted in phosphate-buffered saline, and introduced into the NanoSight NS300 sample chamber via syringe pump. The following script was used for EV measurements: PRIME, DELAY 120, CAPTURE 30, REPEAT 3. Other acquisition settings included the following: camera level, 14; camera shutter speed, 13 milliseconds; camera gain, 360; and laser, blue 488. NTA post-acquisition settings were optimized and kept constant among samples. Software used was NTA version 3.2 Dev. Build 3.2.16.